Check for updates

Increasing the stability of calixarene-capped porous cages through coordination sphere tuning†

Avishek Dey, [ID] [a] Michael R. Dworzak,[a] Kaushalya D. P. Korathotage,[b] Munmun Ghosh,[a] Jahidul Hoq,[b] Christine M. Montone,[b] Glenn P. A. Yap [ID] [b] and Eric D. Bloch [ID] *[a,b]

Chemically and thermally stable permanently porous coordination cages are appealing candidates for separations, catalysis, and as the porous component of new porous liquids. However, many of these applications have not turned to microporous cages as a result of their poor solubility and thermal or hydrolytic stability. Here we describe the design and modular synthesis of iron and cobalt cages where the carboxylate groups of the bridging ligands of well-known calixarene capped coordination cages have been replaced with more basic triazole units. The resultingly higher M−L bond strengths afford highly stable cages that are amenable to modular synthetic approaches and potential functionalization or modification. Owing to the robust nature of these cages, they are highly processable and are isolable in various physical states with tunable porosity depending on the solvation methods used. As the structural integrity of the cages is maintained upon high activation temperatures, apparent losses in porosity can be mediated by resolution and crystallization or precipitation.

Introduction

While recent investigations involving permanently porous cages have demonstrated their utility as a promising class of molecular adsorbents,[1–4] further optimizing the porosity, stability, and processability of porous coordination cages will be vital for realizing their full potential.[5–7] Given their discrete nature, they have unrivaled tunability where their external and internal spaces,[8] structural diversity,[9] and solubility convey added potential for synthesis,[10] purification,[11] and utilization.[12] Although optimization and tuning of the relatively weak intermolecular interactions that govern the solid-state packing and stability of these materials have perhaps been challenging for porosity optimization, it does endow them with an additional level of control for various applications. Optimization of this may afford materials with improved responsiveness to external stimuli[13,14] and allow for extreme structure tuning in, for example, the pursuit of porous liquids.[15,16] Although structure tuning, ligand functionali-

zation, and post-synthetic modification have been leveraged toward these goals,[17–19] the underlying coordination chemistry of these materials is relatively underexplored, particularly as compared to broader classes of porous materials, including MOFs or ZIFs.[20–22]

The development of supramolecular cages, and permanently porous cages more specifically, essentially mirrors the development of MOFs.[23] Where many supramolecular constructs rely on second or third-row metals and neutral donor ligands,[24] the vast majority of cages for which surface areas have been reported, are based on carboxylic acid-type ligands.[4] Among these, both paddlewheel and tetranuclear building units are quite common where both can be incorporated into diverse structure types where overall cage geometry and size can be tuned *via* the bridging ligand or transition metal cations that comprise them. Calixarene-capped cages are featured prominently here and offer the advantage in that they are additionally modifiable at their capping units, which are based on either sulfonylcalix[4]arene (Fig. 1) or thiacalix[4]arene. These structures adopt any one of several structure types depending on ligand used in their syntheses and most commonly present as octahedral cages[25] with ligands situated at their face (tritopic linker) or edge (linear ditopic linker) or as box-like or square structures (bent ditopic linker).[26–28] Both sulfonyl- and thiacalixarene capped cages have been reported for many different transition metal cations[29–33] and their synthesis and assembly is well understood and relatively predictable.[34]

[a]Department of Chemistry & Biochemistry, University of Delaware, Newark, Delaware 19716, USA
[b]Department of Chemistry, Indiana University, Bloomington, Indiana 47405, USA. E-mail: edbloch@iu.edu
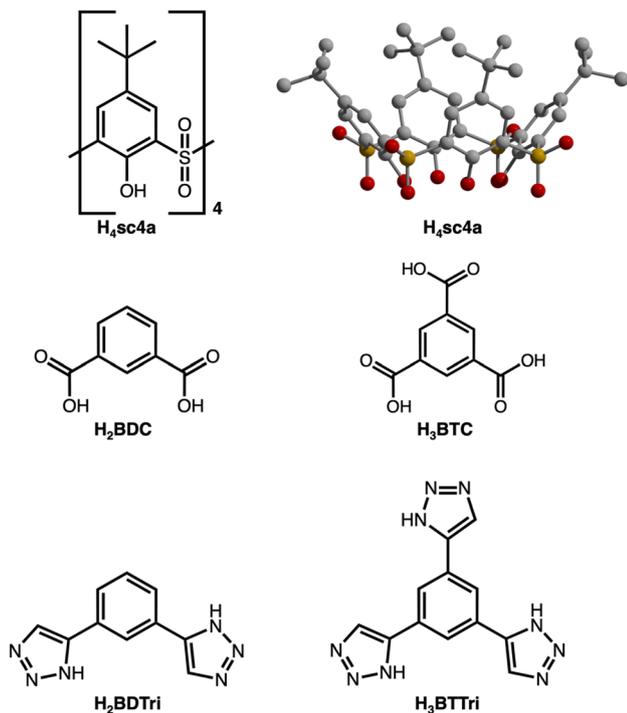
Fig. 1 Capping and bridging ligands used for the synthesis of calixarene-capped cages. Cages based on the sulfonylcalix[4]arene cap (sc4a) have been isolated for isophthalic acid (H$_2$BDC) and trimesic acid (H$_3$BTC) bridging ligands. This work presents the use of triazole-based ligands for the synthesis of highly stable cages.

In an effort to increase the coordination stability of these types of cages, which can still be prone to decomposition *via* hydrolysis, we turned to related families of MOFs that illustrate this concept. Calixarene-capped cages are structurally analogous to a specific pore within PCN-9,[35] a carboxylate-based MOF that is isomorphous to the tetrazole, triazole, and pyrazole-based MOFs M-BTT, M-BTTri, and M-BTP, respectively.[36–38] Ligand tuning was shown to be a viable route toward increasing the stability of these types of MOFs, where anionic N-donor ligands afforded more stable materials as compared to carboxylic acids with stability increasing with pK_a with carboxylate < tetrazolate < triazolate < pyrazolate.[36–38] Toward improving the stability of permanently porous coordination cages, we sought to incorporate triazole or pyrazole groups into otherwise carboxylate-based structures as previous work has established that these types of ligands are compatible with this cage synthesis strategy.[26–28,39]

Results and discussion

Toward the synthesis of so-called Type I, II, or III sulfonylcalix[4]arene-capped cages based on trimesic,[3] terephthalic,[40] and isophthalic acid,[41] respectively, we prepared H$_3$BTTri, and the *para*- and *meta*-isomers of H$_2$BDTri in large quantities *via* established methods. Similarly, the synthesis of sulfonyl[4]calixarene (sc4a) is scalable following established protocols

(Fig. 1).[42,43] Syntheses of cages capped with sc4a or tc4a generally proceed *via* one of three synthetic routes: a one-pot synthesis, pre-reaction of metal with cap or ligand followed by subsequent reaction with remaining ligand or cap, or reaction of the preformed metal building unit—typically as an acetate adduct—with bridging ligands.[34,44] For all three routes, cages can form during solvothermal reaction, cooling the reaction mixture, or layering or diffusion of an anti-solvent into the crude reaction mixture. Although we isolated solids of varying crystallinity, composition, and porosity for a variety of metal salts for all three ligands, we were able to isolate diffraction-quality single crystals for three materials by utilizing solvothermal reaction conditions.

Specifically, the reaction of FeCl$_2$·4H$_2$O with H$_3$BTTri or H$_2$BDTri in DMF at 120 °C for one day, followed by the addition of an ethanoic solution of sc4a, affords a crystalline product in high yield. Single-crystal X-ray diffraction confirms the structure adopts the expected shape in an octahedral cage based on six 4-metal caps terminated by sc4a and connected with 8 BTTri^{3-} ligands at the faces of the octahedron. As expected, given the structural similarities between the analogous MOFs PCN-9 and Mn-BTT,[35,37] the coordination environments of the Fe cations in the structures are similar to our previously reported Fe-calixarene structures based on carboxylic acids and feature pseudooctahedral coordination environments (Table S5†) (Fig. 2). Each iron cation is coordinated to a μ4 species and bridged by two phenolic oxygen atoms, a sulfonyl oxygen, and finally bridged by N atoms from a shared triazole ligand. Although we were unable to refine charge-balancing cations in the structure, the M–L bond distances point to an all Fe(II) cage.[13] Given the slightly elongated linker as compared to H$_3$BTC, this octahedral cap displays longer cap-cap distances along an edge (17.4 vs 14.0 Å). In the solid state, the cages adopt face-to-face packing arrangements where cage–cage interactions are largely governed by *t*Bu–*t*Bu interactions between structures. The cobalt analog of this material, which is isolated under similar, albeit one-pot conditions, has a similar composition and structure. Single-crystal X-ray diffraction shows the structure, [(Co$_4$OHsc4a)$_6$(BTTri)$_8$]$^{6-}$, has a similar unit cell and solid-state packing to the iron structure. This is not entirely unexpected as the metal sites in them are saturated, and the solid-state cage–cage packing is governed by cap–cap interactions.

Although we were unable to obtain diffraction-quality single crystals for the linear ditriazolate ligand, the isophthalic acid analog, 1,3-BDTri, afforded crystalline material upon reaction with CoCl$_2$·6H$_2$O and cap in a DMF : MeOH (3 : 1) ratio after heating at 120 °C for 12 hours. The structure is analogous to the iron and cobalt cages based on H$_3$BTTri, although as a 4-vertex cage, it presents in a box-like or square geometry (Fig. 2). The extended packing of this cage, which crystallizes in P-1, also mirrors that of the analogous H$_2$BDC cage where packing in 2-D is governed by cap–cap interactions, and packing in the third dimension is based on ligand–ligand interactions. The cobalt coordination environment in this structure, [(Co$_4$OHsc4a)$_4$(BDTri)$_8$]$^{4-}$, is essentially identical to
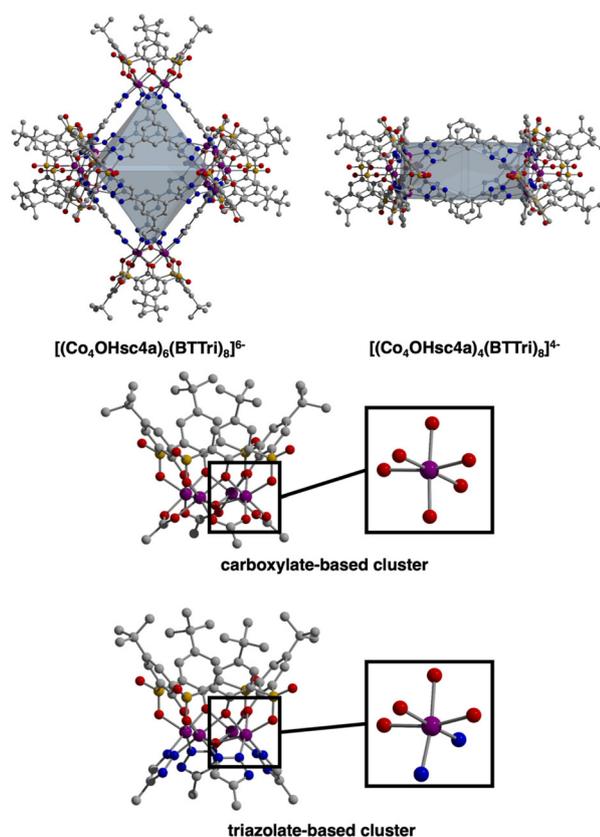
Fig. 2 (Top) Octahedral and box-like cages based on H_3BTTri and H_2BDTri. (Bottom) Comparison between the metal building units in the triazole cages reported here and more typical carboxylate-based building units featured in many calixarene-capped cages.

that in the tristriazoleate-based cage and is isostructural to previously reported tetrazole cages that adopt the same square-like structures.[39]

As is the case for all permanently porous coordination cages, special care during isolation, solvent exchange, and activation must be given to ensure optimal surface area. Initial PXRD patterns confirm the bulk sample, which matches the predicted pattern based on single-crystal analysis, has significant mobility in the solid state upon solvent exchange. Thermogravimetric analysis indicates that after initial mass loss attributed to the evacuation of pore-bound solvent, all three materials display no further mass loss until at least 400 °C. Although this gives no indication of porosity after heating to elevated temperatures, it confirms the enhanced structural stability of these cages as compared to carboxylate-based analogs. In order to optimize the surface area for these materials, we screened exchange solvents as the cages have moderate to good solubility in a number of organic solvents. Ultimately, room temperature methanol exchanges followed by heating under flowing N_2 or dynamic vacuum afforded samples with the highest porosities. Under these conditions, we recorded N_2 accessible BET (Langmuir) surface areas of 581 (919), 559 (1067), and 307 (616) m^2 g^{-1} for

$[(Fe_4OHsc4a)_6(BTTri)_8]^{6-}$, $[(Co_4OHsc4a)_6(BTTri)_8]^{6-}$, and $[(Co_4OHsc4a)_4(BDTri)_8]^{4-}$, respectively. These values are higher than those reported for most H_3BTC or H_2BDC cages capped with sc4a, whose BET surface areas are typically 200–300 m^2 g^{-1}. This is likely a result of the slightly expanded pore volumes of the triazole cages as compared to the carboxylate structures.

To further investigate the stability that was possibly evidenced by the TGA profiles, we initiated a detailed study targeting solvation and thermal stability. As the cobalt cages had limited solubility, we focused on the iron-based cage $[(Fe_4OHsc4a)_6(BTTri)_8]^{6-}$. It has appreciable solubility in dichloromethane, chloroform, dimethylacetamide, acetone, and ethyl acetate. To further elucidate thermal stability, TGA data were collected at 5 °C min^{-1} ramp rates to 100, 200, 300, 400, 500, and 600 °C for six different samples. Although the TGA curves for these samples were essentially identical and only show mass losses as a function of temperature, IR spectra on materials after the heating phases confirm that only minor compositional variations are obvious after heating to 400 °C (Fig. 3).

While the complement of TGA and IR suggested minimal cage degradation up to at least 400 °C activation temperatures, cage packing in the solid state, and thus porosity, may be impacted by heating. A thorough activation screen confirms that although the cage has an optimal activation temperature of 150 °C, it maintains porosity at elevated heating, where the Langmuir surface area of 858 m^2 g^{-1} decreases to 689, 634, 433, and 389 m^2 g^{-1} after heating to 200, 250, 300, or 400 °C, respectively. A prime example of the benefits of cage solution processability is given here as samples with diminished porosity as a result of overheating can simply be recrystallized from
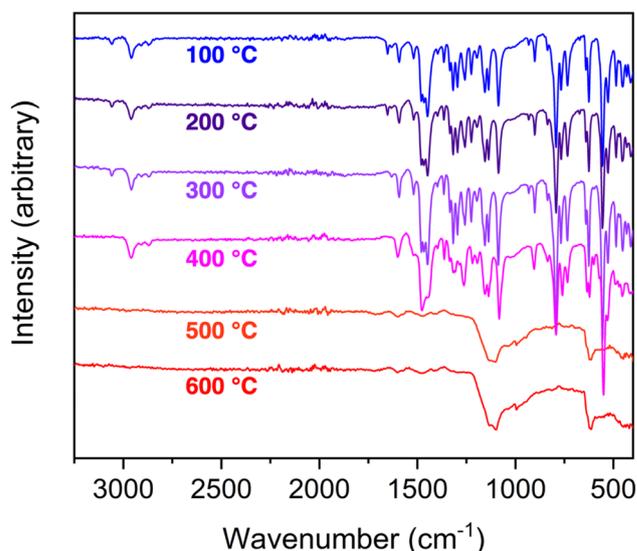

Fig. 3 Infrared spectra collected for $[(Fe_4OHsc4a)_6(BTTri)_8]^{6-}$ as a function of activation temperature. Consistent with TGA data, the cage displays minimal structural degradation up to an activation temperature of at least 400 °C.

volatile solvent to restore the 3-D packing of the cages. A relatively rapid recrystallization of a thermally-degraded sample ($\sim$200 m^2 g^{-1}) from chloroform and subsequent heating to 150 °C actually affords a slightly higher surface area than the starting sample with 626 (929) *vs.* 581 (919) m^2 g^{-1}. Interestingly, recrystallization of an as-synthesized sample from chloroform, followed by activation at 150 °C, affords a significantly lower surface area of 216 (436) m^2 g^{-1}. Recrystallization from acetone, dichloromethane, or ethyl acetate all gave samples with lower surface areas.

In addition to solid-state stability, the solvent processability and stability of these cages can even aid in characterization as MALDI was used to confirm the presence of the cage, the first time mass spectrometry was used for calixarene-capped cages (Fig. S15†). The cages also display good hydrolytic stability with no dissolution or decomposition after boiling in water for one week, although the surface areas of samples treated in this manner are typically $\sim$10–15% lower than starting cages.

Conclusions

In conclusion, this work has shown that a class of highly stable, permanently microporous cages can be prepared *via* utilization of the isoreticular design principles that are a hallmark of MOF and ZIF chemistry. The triazolate-based cages reported here boast excellent thermal and hydrolytic stability while maintaining the solution processability of molecular adsorbents. Importantly, when apparent porosity is lost as a result of excessive thermal treatment, it can be regained *via* simple recrystallization methods as the parent cages persist in the solid state and their three-dimensional packing is tunable in a post-synthesis manner. Finally, we envision that further functionalization of these types of cages through, for example, 5-position modification of H$_3$BDTri, can afford new highly tunable, stable, and processable molecular adsorbents.

Conflicts of interest

There are no conflicts to declare.

Acknowledgements

References

1 M. A. Little and A. I. Cooper, *Adv. Funct. Mater.*, 2020, **30**, 1909842.

2 T. Hasell and A. I. Cooper, *Nat. Rev. Mater.*, 2016, **1**, 16053.

3 F.-R. Dai and Z. Wang, *J. Am. Chem. Soc.*, 2012, **134**, 8002–8005.

4 A. J. Gosselin, C. A. Rowland and E. D. Bloch, *Chem. Rev.*, 2020, **120**, 8987–9014.

5 H. Furukawa, K. E. Cordova, M. O'Keeffe and O. M. Yaghi, *Science*, 2013, **341**, 123044.

6 M. Yoshizawa, J. K. Klosterman and M. Fujita, *Angew. Chem., Int. Ed.*, 2009, **48**, 3418–3438.

7 P. Mal, B. Breiner, K. Rissanen and J. R. Nitschke, *Science*, 2009, **324**, 1697.

8 M. T. Yong, O. M. Linder-Patton and W. M. Bloch, *Inorg. Chem.*, 2022, **61**, 12863–12869.

9 H. Lin, Z. Xiao, K. N. Le, T.-H. Yan, P. Cai, Y. Yang, G. S. Day, H. F. Drake, H. Xie, R. Bose, C. A. Ryan, C. H. Hendon and H.-C. Zhou, *Angew. Chem., Int. Ed.*, 2022, **61**, e202214055.

10 A. Khobotov-Bakishev, L. Hernandez-Lopez, C. von Baeckmann, J. Albalad, A. Carne-Sanchez and D. Maspoch, *Adv. Sci.*, 2022, **9**, 2104753.

11 A. M. Antonio, K. J. Korman, G. P. A. Yap and E. D. Bloch, *Chem. Sci.*, 2020, **11**, 12540–12546.

12 A. M. Antonio, K. J. Korman, M. M. Deegan, G. A. Taggart, G. P. A. Yap and E. D. Bloch, *Inorg. Chem.*, 2022, **61**, 4609–4617.

13 M. M. Deegan, T. S. Ahmed, G. P. A. Yap and E. D. Bloch, *Chem. Sci.*, 2020, **11**, 5273–5279.

14 S. Bera, K. Dey, T. K. Pal, A. Halder, S. Tothadi, S. Karak, M. Addicoat and R. Banerjee, *Angew. Chem.*, 2019, **131**, 4287–4291.

15 L. Ma, C. J. E. Haynes, A. B. Grommet, A. Walczak, C. C. Parkins, C. M. Doherty, L. Longley, A. Tron, A. R. Stefankiewicz, T. D. Bennett and J. R. Nitschke, *Nat Chem.*, 2020, **12**, 270–275.

16 M. Mastalerz, *Nature*, 2015, **527**, 174.

17 J.-R. Li, A. A. Yakovenko, W. Lu, D. J. Timmons, W. Zhuang, D. Yuan and H.-C. Zhou, *J. Am. Chem. Soc.*, 2010, **132**, 17599–17610.

18 A. Carne-Sanchez, J. Albalad, T. Grancha, I. Imaz, J. Juanhuix, P. Larpent, S. Furukawa and D. Maspoch, *J. Am. Chem. Soc.*, 2019, **141**, 4094–4102.

19 M. R. Dworzak, C. M. Montone, N. I. Halaszynski, G. P. A. Yap, C. J. Kloxin and E. D. Bloch, *Chem. Commun.*, 2023, **59**, 8977–8980.

20 M. J. Kalmutzki, N. Hanikel and O. M. Yaghi, *Sci. Adv.*, 2018, **4**, eaat9180.

21 M. Ding, X. Cai and H.-L. Jiang, *Chem. Sci.*, 2019, **10**, 10209–10230.

22 K. S. Park, Z. Ni, A. P. Cote, J. Choi, R. Huang, F. J. Uribe-Romo, H. K. Chae, M. O'Keeffe and O. M. Yaghi, *Proc. Natl. Acad. Sci. U. S. A.*, 2006, **103**, 10186–10191.

23 X. Zhang, Z. Chen, X. Liu, S. L. Hanan, X. Wang, R. Taheri-Ledari, A. Maleki, P. Li and O. K. Farha, *Chem. Soc. Rev.*, 2020, **49**, 7406–7427.

24 S. Pullen, J. Tessarolo and G. H. Clever, *Chem. Sci.*, 2021, **12**, 7269–7293.

25 K. Xiong, F. Jiang, Y. Gai, D. Yuan, L. Chen, M. Wu, K. Su and M. Hong, *Chem. Sci.*, 2012, **3**, 2321–2325.

26 K. Xiong, F. Jiang, Y. Gai, Z. He, D. Yuan, L. Chen, K. Su and M. Hong, *Cryst. Growth Des.*, 2012, **12**, 3335–3341.

27 C.-M. Liu, D.-Q. Zhang, X. Hao and D.-B. Zhu, *Eur. J. Inorg. Chem.*, 2012, **26**, 4210.

28 K. Li and W. Liao, *CrystEngComm*, 2020, **22**, 7668–7672.

29 F.-R. Dai, Y. Qiao and Z. Wang, *Inorg. Chem. Front.*, 2016, **3**, 243–249.

30 M. Liu, W. Liao, C. Hu, S. Du and H. Zhang, *Angew. Chem., Int. Ed.*, 2012, **51**, 1585–1588.

31 S. Du, C. Hu, J.-C. Xiao, H. Tan and W. Liao, *Chem. Commun.*, 2012, **48**, 9177–9179.

32 M. Liu, S. Du and W. Liao, *J. Mol. Struct.*, 2013, **1049**, 310–314.

33 M. Liu and W. Liao, *CrystEngComm*, 2012, **14**, 5727–5729.

34 Y. Bi, S. Du and W. Liao, *Coord. Chem. Rev.*, 2014, **276**, 61–72.

35 S. Ma and H.-C. Zhou, *J. Am. Chem. Soc.*, 2006, **128**, 11734–11735.

36 V. Colombo, S. Galli, H. J. Choi, G. D. Han, A. Maspero, G. Palmisano, N. Masciocchi and J. R. Long, *Chem. Sci.*, 2011, **2**, 1311–1319.

37 M. Dinca, A. Dailly, Y. Liu, C. M. Brown, D. A. Neumann and J. R. Long, *J. Am. Chem. Soc.*, 2006, **128**, 16876–16883.

38 T. M. McDonald, D. M. D'Alessandro, E. Krishna and J. R. Long, *Chem. Sci.*, 2011, **2**, 2022–2028.

39 X. Hang, X. Wang, M. Wang, M. Chen and Y. Bi, *Inorg. Chem. Front.*, 2023, **10**, 926–933.

40 F.-R. Dai, U. Sambasivam, A. J. Hammerstrom and Z. Wang, *J. Am. Chem. Soc.*, 2014, **136**, 7480–7491.

41 F.-R. Dai, D. C. Becht and Z. Wang, *Chem. Commun.*, 2014, **50**, 5385–5387.

42 H. Kumagi, M. Hasegawa, S. Miyanari, Y. Sugawa, Y. Soto, T. Hori, S. Ueda, H. Kamiyama and S. Miyano, *Tetrahedron Lett.*, 1997, **38**, 3971–3972.

43 N. Iki, H. Kumagai, N. Morohashi, K. Eijma, M. Hasegawa, S. Miyanari and S. Miyano, *Tetrahedron Lett.*, 1998, **39**, 7559–7562.

44 M. R. Dworzak, M. M. Deegan, G. P. A. Yap and E. D. Bloch, *Inorg. Chem.*, 2021, **60**, 5607–5616.